Quantum Confinement Regimes in CdTe Nanocrystals Probed by Single Dot Spectroscopy: From Strong Confinement to the Bulk Limit

Jenya Tilchin,[†] Freddy T. Rabouw,[‡] Maya Isarov,[†] Roman Vaxenburg,[†] Relinde J. A. Van Dijk-Moes,[‡] Efrat Lifshitz,[*,†] and Daniel Vanmaekelbergh[*,‡]

[†]Schulich Faculty of Chemistry, Russell Berrie Nanotechnology Institute, Solid State Institute, Technion—Israel Institute of Technology, Haifa 32000, Israel and [‡]Debye Institute of Nanomaterials Science, University of Utrecht, Utrecht 3508 TA, The Netherlands

ABSTRACT Sufficiently large semiconductor nanocrystals are a useful model system to characterize bulk-like excitons, with the electron and hole bound predominantly by Coulomb interaction. We present optical characterization of excitons in individual giant CdTe nanocrystals with diameters up to 25.5 nm at 4.2 K under varying excitation power and magnetic field strength. We determine values for the biexciton binding energy, diamagnetic shift constant, and Landé *g*-factor, which approach the bulk values with increasing nanocrystal size.

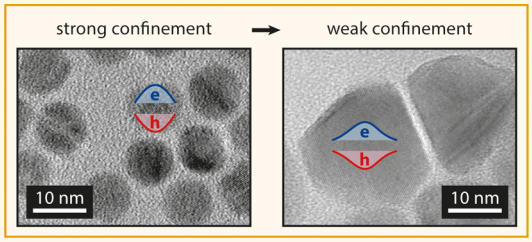

KEYWORDS: semiconductor quantum dots · weak quantum confinement · exciton localization · multiexcitons

Colloidal semiconductor nanocrystals (NCs) have raised much scientific interest during the past three decades, due to the possibility of tuning their optoelectronic properties[1−3] by controlling size, shape and composition. Previous research was mainly focused on the regime of strong spatial quantum confinement, where the NC radius is smaller than the exciton Bohr radius. In this regime, the discrete electron (hole) energy level structure is governed by the NC size/shape and the dielectric properties of the surroundings. Advances in colloidal chemistry have led to synthesis protocols for NCs with dimensions in the strong confinement regime with tunable, nearly monochromatic emission from the lowest exciton state.[4−6] The electronic structure of these systems has been studied in detail in ensembles, and at the single NC level using scanning tunneling microspectroscopy and (time-resolved) optical spectroscopy. The results have been compared to advanced theoretical calculations.

Larger colloidal nanocrystals showing marginal quantum confinement[7] have not been fully explored, although these systems display a feature that could make them particularly interesting for basic science. An electron−hole pair in a large NC is bound almost entirely by Coulomb attraction, and in this respect resembles an exciton in a bulk crystal. Excitons in bulk semiconductors have been extensively studied. However, in bulk crystals the exciton can diffuse over considerable distances until it binds to a crystal defect or atomic impurity. Generally, the wavelength of emission by the resulting bound exciton is different from the free exciton, and depends on the type of impurity to which it is bound. This can complicate the interpretation of the photoluminescence (PL) spectra in bulk crystals. Large colloidal nanocrystals provide a bulk-like crystal environment for excitons while limiting long distance diffusion, and may be a valuable alternative platform to study the PL of bulk-like excitons.

Here, we report on microphotoluminescence (μ-PL) spectroscopy of individual CdTe nanocrystals, passivated with a two monolayer thick shell of CdSe. We performed experiments at cryogenic temperatures and at a varying external magnetic field (**B**-field) of up to 5 T. The NCs under study have a diameter ranging from 9 to

* Address correspondence to ssefrat@technion.ac.il, d.vanmaekelbergh@uu.nl.

Received for review April 30, 2015 and accepted July 16, 2015.

Published online July 16, 2015
10.1021/acsnano.5b02597

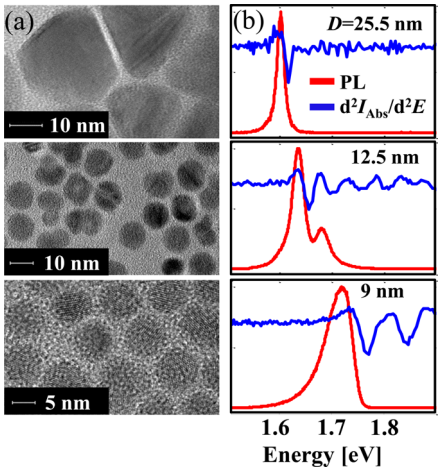

Figure 1. (A) TEM images and (B) ensemble photoluminescence (red) and second derivative absorption spectra (blue) recorded at 4.2 K of the three CdTe NC batches investigated; from top to bottom, samples 9, 12.5, and 25.5 nm.

25.5 nm. Since the Bohr exciton radius in CdTe is 9 nm, these nanocrystals should feature intermediate to weak quantum confinement. In the largest nanocrystals, the emission energy approaches the free-exciton emission of macroscopic CdTe.[8] We distinguish the regimes of a single and biexcitons, and determine the biexciton binding energy. We calculate the diamagnetic shifts and the Landé *g*-factors from the Zeeman splitting and energy shifts of the lines in the exciton fine structure as a function of the applied **B**-field. Our work shows that physical parameters such as the exciton energy, the biexciton binding energy, the diamagnetic shift, and the Landé *g*-factor are strongly size-dependent. They approach the values reported for bulk CdTe in the largest NCs examined.

RESULTS AND DISCUSSION

We studied three batches of CdTe/CdSe core/shell NCs, with total diameters of 9, 12.5, and 25.5 nm and size dispersion about 10% (denoted, from here on, as sample 9 nm, sample 12.5 nm, and sample 25.5 nm, respectively). The synthesis of CdTe/CdSe core/shell NCs (denoted from here on as CdTe) is described in the Supporting Information. Transmission electron microscopy (TEM, Figure 1A) shows that the small and intermediate nanocrystals have a nearly spherical shape, while crystals of sample 25.5 nm are more tetrahedral, typical for zinc blende CdTe.

The ensemble photoluminescence (red line) and second derivative absorption spectra (blue line) recorded at cryogenic temperatures are given in Figure 1B. The second derivative absorption curves of the CdTe of samples 9 and 12.5 nm exhibit pronounced minima originating from the discrete exciton transitions. The second derivative absorption curve of the sample 25.5 nm shows the lowest energy transition at 1.618 eV, and the luminescence peak is centered around 1.605 eV. As a comparison, the emission energy of the lowest-energy free exciton in bulk CdTe has been reported to be 1.597 eV at 1.6 K[9] or 1.596 eV at 4.2 K.[8] The blue-shift of the emission in our NCs compared to bulk CdTe can be attributed to quantum confinement of the exciton wave function, but is very small (<10 meV). The full-width-half-maximum (fwhm) of the lowest exciton transition in both absorption and PL of the largest NCs is substantially smaller than that observed for the smaller CdTe NCs, and the same holds for the Stokes shift between the absorption and luminescence peaks. These data demonstrate that the exciton in CdTe NCs of sample 25.5 nm has a close to bulk-type character.

Exceptional behavior is seen in the PL of sample 12.5 nm in Figure 1B. There are two distinct emission bands separated by 45 meV. This separation is similar to the gap between the first and the second transition in the absorption spectrum (blue line). A tentative explanation for the high-energy emission would be radiative decay of an excited exciton state. NCs in the intermediate confinement regime might have suppressed cooling of hot-carrier states, because of a bottleneck for cooling *via* phonon coupling, while the electron and hole are sufficiently delocalized to have reduced Auger coupling[10] but sufficiently far from the NC surface to avoid strong coupling to ligand vibrations.[11] More in-depth experiments are required to confirm this assignment of the high-energy emission band in our sample.

Figure 2A demonstrates a typical evolution of the zero **B**-field μ-PL spectra with increasing excitation power, obtained on an individual CdTe NC of sample 25.5 nm at cryogenic temperature.[12,13] The excitation power of each spectrum is indicated. The spectra were recorded one directly after the other, each with an acquisition time of 100 s. The intensity trace of Figure 2B reveals rare occasions of intermittency, as well as some jittering around a central emission band maximum, proof that a single NC is examined. Intensity intermittency as observed in Figure 2B has previously been ascribed to photocharging and Auger quenching,[1,14−16] or to temporary diffusion of a charge to surface or ligand sites.[17,18]

The emission spectra in Figure 2A display multiple bands presumably originating from single and multiexciton states. At the lowest excitation power, the μ-PL spectrum is dominated by single-exciton emission (X; blue lines are Gaussian fits) centered at 1.6114 eV, with a characteristic fwhm of ~800 μeV. The broadening of the exciton line may be related to the remaining minor jittering[19,20] and coupling to acoustic phonons.[21,22] Upon increase of the excitation power, new bands emerge, both at lower energy and at higher energy than X. In our measurements, the estimated number of excitons per NC in the steady state ranges from 0.11 to 1.53, as indicated in the plots (see Supporting Information for the calculation).

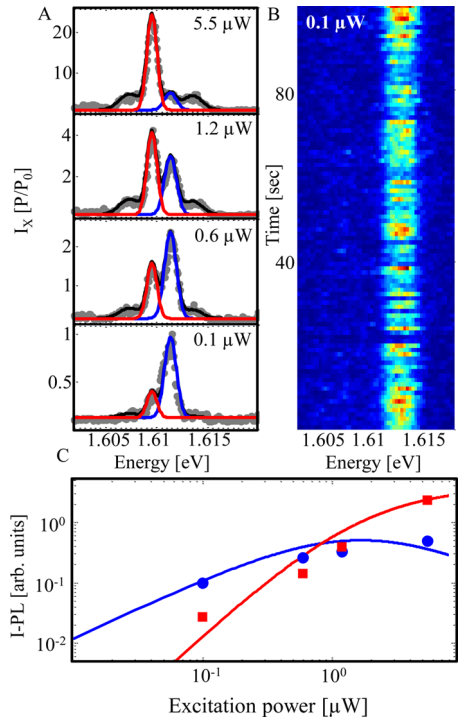

Figure 2. (A) PL spectra of an individual NC of sample 25.5 nm, recorded under different excitation powers. We observe emission from the ground state single exciton (X; blue), and at higher powers also from the biexciton states (XX; red). The spectra are normalized to the peak intensity of the X emission at the lowest excitation power. The excitation power of each spectrum is shown. Integration times are 100 s. The steady-state exciton population under continuous-wave excitation is estimated as described in the Supporting Information. (B) A time trace of the PL emission with P = 0.1 μW, and a time binning of 1 s. (C) Integrated intensity (symbols) and theoretical population of the X and XX (solid lines) *versus* excitation power, on a double-logarithmic scale and color coded as in (A).

The emission band centered at 1.6096 eV, which is the strongest at excitation powers higher than 1 μW, is attributed to the biexciton (XX; red lines are Gaussian fits). Plots of the integrated intensity of X and XX (red and blue symbols) *versus* the excitation power are shown in Figure 2C. The general trends of population distribution *versus* excitation power (red and blue solid lines) were calculated according the procedure given in literature,[13,23] as described in the Supporting Information. The lowest power of 0.1 μW is in the regime without saturation of the populations of single and biexciton. At higher powers, however, the actual populations deviate from the purely linear and quadratic trends, indicating that the system saturates in the highest excited state considered in our model (*i.e.*, XX). Comparison of the experimental intensities (symbols in Figure 2C) to the simulated populations (solid lines in Figure 2C) supports our assignment that the band at 1.6114 eV originates from X (blue in Figures 2A,C), and the one at 1.6096 eV from XX (red). The other emission bands at higher and lower energy (black), which appear at the highest excitation powers, might be related to triexciton states or to intermittent charging. Indeed, the charged single exciton can yield red-shifted emission with respect to the neutral exciton,[24] while the charged biexciton or the triexciton can yield blue-shifted emission.[25]

TABLE 1. Experimental Biexciton Binding Energies ($E^{XX}_{Binding}$) of the Samples under Investigation

D_{NC} [nm]	9	12.5	25.5
$E^{XX}_{Binding}$ (experimental) [meV]	3.4—5	2.8	1.8
$E^{XX}_{Binding}$ (calculated) [meV]	4.7	3	1.3

From the energy separation between X (blue) and XX (red) emission lines, we determine the XX binding energy ($E^{XX}_{Binding}$). The binding energies of the various multiexciton states in a NC are determined by many-body Coulomb interactions. We estimate the expected values for $E^{XX}_{Binding}$ from the single-particle states, as the first-order energy correction due to Coulomb interactions between pairs of charge carriers (see Supporting Information).[13] It should be noted that energy corrections due to polarization of the single-carrier wave functions and electron−hole correlation become of increasing importance for the largest NC sizes. Our perturbative first-order calculations should therefore be regarded as estimates for the biexciton binding energy, while only advanced calculations accounting for electron−hole configuration interaction[26] can quantitatively predict the energies. Table 1 compares the theoretical and the experimental values for the $E^{XX}_{Binding}$, for the three NC sizes investigated. Theory and experiment agree on the trend that $E^{XX}_{Binding}$ is larger in smaller NCs.

The bottom panel of Figure 3A shows typical emission spectra of the X band of an individual CdTe NC of sample 9 nm. The black curves are the nonpolarized spectra. They have an anisotropic shape leaning to lower energies, which we ascribe to coupling to longitudinal acoustic phonon modes.[22,27] Blue and red lines depict the linear polarization components, recorded with and without **B**-field. The peak positions for the two components are slightly but clearly separated with respect to one another. At 0 T, the separation is ~0.3 meV, while at increasing magnetic field strength, the separation increases (0.47 meV at 4 T). The top panel of Figure 3A displays the circularly polarized components of the same NC. In contrast to the linear components (Figure 3A; bottom), the two circular components lie at roughly equal energies.

Figure 3B shows the nonpolarized emission spectra (black curves) of X from a single NC of sample 25.5 nm, at different **B**-field strengths. The polarized components in these spectra were difficult to resolve, because they are even closer than in the smaller NCs. However, the shape of the spectra is similar to that measured for the smaller NCs (Figure 3A), suggesting that two slightly separated linear components are present.

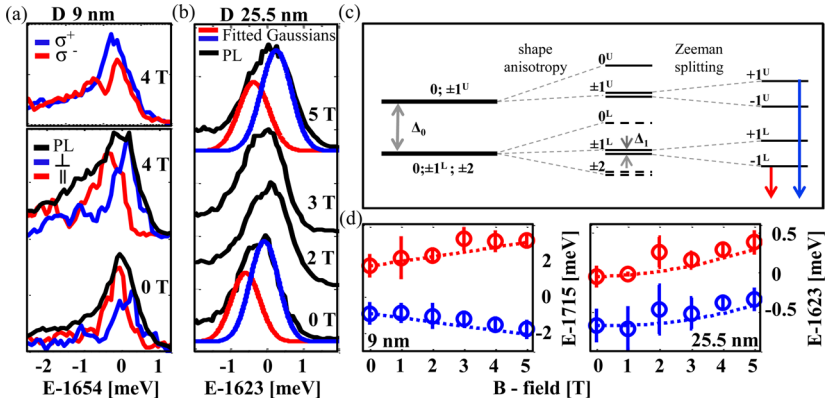

Figure 3. (A) Polarization resolved X band μ-PL spectra of sample 9 nm. Bottom panel: parallel/perpendicular (red/blue lines) and nonpolarized (black) μ-PL spectra recorded at 0 T (bottom) and 4 T (top) magnetic field. Top panel: circular polarization resolved μ-PL spectra recorded at 4 T magnetic field. (B) Nonpolarized μ-PL spectra of an individual CdTe NC of sample 25.5 nm (black) recorded at different powers of B-field. The excitonic band was fitted to two Gaussians representing the high- and low-energy components associated with the Zeeman splitting. (C) Schematic representation of exciton fine structure. (D) The peak energy of each component *versus* strength of B-field for single NCs of samples 9 nm (left) and 25.5 nm (right) color coded as in (A). The dashed lines present the fitted magnetic field dependent behavior according to eq 1.

To determine the peak positions of these, we fit two Gaussians to the spectra (red and blue curves).

Linear and/or circular polarization of excitonic emission of II−VI NCs occurs due to existence of different X states, characterized by different total angular momentum and projection. The X states are split in energy primarily due to electron−hole exchange interaction, a noncentrosymmetric crystal structure, and deviations from a spherical NC shape.[1,28] Figure 3C schematically depicts the X energy levels. On the left, we depict the energy levels in a perfectly spherical crystal in the absence of a **B**-field: two manifolds separated by electron−hole exchange over a gap Δ_0.[29] We estimate (see Supporting Information) that the value of Δ_0 (~0.3 meV) for sample 9 nm is of the order of k_BT even at cryogenic temperatures, indicating that all X states are thermally populated. When corrections due to shape anisotropy are also taken into account, the manifolds split (see Figure 3C). Of the resulting states, only the $|\pm1^U\rangle$, $|\pm1^L\rangle$ and $|0^U\rangle$ states are "bright", *i.e.*, the transition to the NC ground state is electric dipole allowed. We restrict our discussion to the emitting states that undergo Zeeman splitting in an external **B**-field, *viz.* $|\pm1^U\rangle$ and $|\pm1^L\rangle$, because at low **B**-field Zeeman splitting of these states is the dominant field-dependent effect on the emission spectra. Distortion of the NC shape from a cylindrical symmetry (see Figure 1A) splits each of these two bright states into substates which carry perpendicular linear polarizations of their emission lines with an energy separation of Δ_1.[22] Thus, the splitting of linear polarization components at zero-field reflects the splitting of each of $|\pm1^U\rangle$ and $|\pm1^L\rangle$. In a cylindrically symmetric NC, the application of a magnetic field would Zeeman split the $|\pm1\rangle$ states in $|+1\rangle$ and $|-1\rangle$ components with purely circularly polarized emission. In our experiment, the low-symmetry shape of the NCs, combined with effects of the close energy separation of the emitting states, jittering and a limited spectral resolution, results in the observation of an effective elliptical polarization (compare the linear and circular polarization resolved detection at 4 T of the 9 nm sample in Figure 3A). From here on, we focus our discussion on the linear component of the elliptical polarization. We propose that the experimental splitting of the linear components at higher magnetic fields (Figure 3A bottom panel) is related to the Zeeman shift of outer bright states $|+1^U\rangle$ and $|-1^L\rangle$ (red and blue arrows in Figure 3C). The inner bright states $|-1^U\rangle$ and $|+1^L\rangle$ contribute to the emission intensity at the overlap region between the two polarization peaks, but the polarization of individual lines cannot be resolved. Important to mention, at zero **B**-field the angle-of-appearance of X emission orthogonal polarized components depends on the angle of appearance of the in-plane projection of the shape asymmetry direction,[28] as shown in the Supporting Information.

Figure 3D, right panel, shows how the peak energies of the low-energy (blue) and high-energy (red) components in the emission spectra of Figure 3B shift with increasing **B**-field strength. The parameters g_X and γ_2 were extracted from the experimental data (see Supporting Information) using the following relation:

$$E^{\pm}(B) = E_0^{\pm} \pm \frac{1}{2} g_X \mu_B B + \gamma_2 B^2 \qquad (1)$$

for the high-energy (+) and the low-energy (−) components. The first term in eq 1 is the energies of the bright states $|+1^U\rangle$ and $|-1^L\rangle$ at zero-field. The second term, linear with the magnetic field strength, describes Zeeman splitting. The third term accounts for the diamagnetic shift (γ_2), which has a quadratic dependence on the magnetic field strength. In eq 1, we have assumed that the $|\pm1^U\rangle$ and $|\pm1^L\rangle$ states have equal

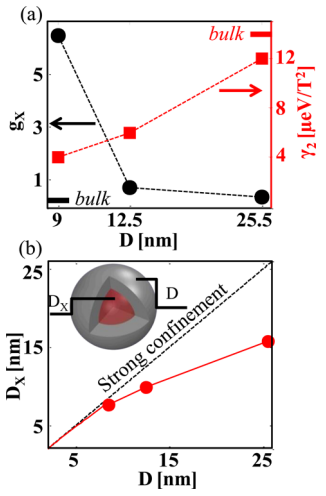

Figure 4. (A) Black circles: extracted Landé *g*-factor (g_X), left abscissa. Red squares: extracted diamagnetic shift (γ_2), right abscissa *versus* NC size. The bulk values of g_X and γ_2 are presented as horizontal black and red lines, respectively, on abscissa. (B) Schematics of the exciton diameter (D_X) *versus* NC diameter (D). The diagonal black dashed line represents the linear dependence of D_X on D (strong confinement); red circles: experimental D_X showing the deviation form linear dependence on D due to Coulomb attraction of the electron−hole pair (weak confinement regime).

Landé *g*-factors (g_X), *i.e.*, the Zeeman splittings have equal magnitudes.

The open circles in Figure 3D show the maxima of the fitted Gaussians and the dashed lines are plots of eq 1 using the best fitted values for the parameters g_X and γ_2. Special attention should be paid to the qualitatively different trends for the two different NC sizes. For the small NC (sample 9 nm; left), the two components in the emission spectrum become further separated upon increasing the magnetic field, while for the large NC (sample 25.5 nm; right), both components shift to higher energy but they hardly split further. This indicates that the Zeeman effect dominates the influence of the magnetic field on the small NC, while the large NC is most strongly affected by the diamagnetic shift.

Figure 4A shows plots of the extracted values for g_X and γ_2 *versus* NC size. There are clear trends that g_X decreases with increasing NC size,[30] while γ_2 increases. In fact, the values approach those for bulk CdTe[31] (g_X = 0.35 and γ_2 = 14.7 μeV/T^2) in the largest NC sample investigated.

From the diamagnetic shift, we can estimate the extent of exciton confinement in the NCs. According to the model presented by Walck *et al.*,[32] γ_2 is to a good approximation equal to $\gamma_2 = e^2\langle r_X^2\rangle/8\mu$ where e is the electron charge, μ is the reduced mass of the exciton, and $\langle r_X^2\rangle^{1/2}$ is the radius of the exciton. Thus, the effective exciton diameter (D_X) is equal to $D_X = 2\langle r_X^2\rangle^{1/2}$.

Figure 4B shows that the estimated size D_X of the exciton does in fact not increase linearly with the physical size D of the nanocrystal. The ratio D_X/D decreases from 0.9 in the smallest NCs investigated to 0.62 for the largest NCs. This points directly to exciton localization under weak spatial confinement due to the influence of Coulomb interaction. The exciton is localized to a size that is substantially smaller than the physical size of the NCs. It has been shown theoretically[7] that these excitons are focused at the central part of the NC, maintaining a uniform dielectric environment. Such configuration resembles a self-assembled quantum dot within a semiconductor host, and approaches the behavior of excitons in bulk semiconductors. The influence of the exterior surfaces can therefore be expected to be substantially reduced, which would explain the remarkable spectral stability of the exciton emission over 100 s (Figure 2B).

CONCLUSION

To summarize, we have examined single and multi-excitons in CdTe NCs with sizes ranging from the strong to the weak confinement regime. The properties of the exciton extracted for NCs in the weak confinement regime approach those of bulk CdTe. Colloidal nanocrystals of increasing size up to tens of nanometers diameter form a suitable platform to study how the exciton fine structure changes gradually with the degree of quantum confinement, from the regime of strong confinement to the regime where excitons exist by virtue of the Coulomb attraction.

METHODS

The μ-PL spectra of single NCs were recorded using a fiber-based confocal microscope with NA = 0.65 immersed in a cryogenic system.[12,13] The NCs were dispersed over a silicon substrate with a density <1 NC/μm^2 and were excited by a continuous wave diode laser (E_{exc} = 1.87 eV) with diffraction limited fwhm spot of ~0.7 μm and a spectral resolution of 300 μeV. For each batch of CdTe NCs, a few tens of individual NCs were examined at cryogenic temperatures. We present results using different excitation intensities, a variable **B**-field between 0 and 5 T, and polarization-sensitive detection of the linear and circular components of the exciton emission.

Conflict of Interest: The authors declare no competing financial interest.

Acknowledgment. This research was supported by the Volkswagen Stiftung, (Project No. 88116), the Israel Science Foundation (Project No. 985/11), the Israel Science Foundation, Bikura (Project No. 1425/04) and the German Israel Foundation (Project No. 156/03-12.6). F.T.R. and D.V. acknowledge funding by the "Foundation for Fundamental Research on Matter (FOM)", which is financially supported by the "The Netherlands Organization for Scientific Research (NWO)".

Supporting Information Available: Additional information for synthesis of NCs; electron diffraction pattern of the studied NCs; calculation of multiexciton populations, band structure, exciton binding energy, exchange interaction, Zeeman split, and diamagnetic shift constants. The Supporting Information is available free of charge on the ACS Publications website at DOI: 10.1021/acsnano.5b02597.

REFERENCES AND NOTES

1. Efros, A. L.; Rosen, M.; Kuno, M.; Nirmal, M.; Norris, D. J.; Bawendi, M. Band-Edge Exciton in Quantum Dots of Semiconductors with a Degenerate Valence Band: Dark and Bright Exciton States. *Phys. Rev. B: Condens. Matter Mater. Phys.* **1996**, *54*, 4843–4856.
2. Piryatinski, A.; Ivanov, S. A.; Tretiak, S.; Klimov, V. I. Effect of Quantum and Dielectric Confinement on the Exciton-Exciton Interaction Energy in Type II Core/Shell Semiconductor Nanocrystals. *Nano Lett.* **2007**, *7*, 108–115.
3. Frantsuzov, P.; Kuno, M.; Janko, B.; Marcus, R. A. Universal Emission Intermittency in Quantum Dots, Nanorods and Nanowires. *Nat. Phys.* **2008**, *4*, 519–522.
4. Rubin-Brusilovski, A.; Maikov, G.; Kolan, D.; Vaxenburg, R.; Tilchin, J.; Kauffmann, Y.; Sashchiuk, A.; Lifshitz, E. Influence of Alloying on the Optical Properties of IV−VI Nanorods. *J. Phys. Chem. C* **2012**, *116*, 18983–18989.
5. Ithurria, S.; Tessier, M. D.; Mahler, B.; Lobo, R. P. S. M.; Dubertret, B.; Efros, A. L. Colloidal Nanoplatelets with Two-Dimensional Electronic Structure. *Nat. Mater.* **2011**, *10*, 936–941.
6. Alivisatos, A. P. Semiconductor Clusters, Nanocrystals, and Quantum dots. *Science* **1996**, *271*, 933–937.
7. Efros, A. L.; Efros, A. L. Interband Absorption of Light in a Semiconductor Sphere. *Sov. Phys. Semicond.* **1982**, *16*, 772–775.
8. Horodyský, P.; Hlídek, P. Free-Exciton Absorption in Bulk CdTe: Temperature Dependence. *Phys. Status Solidi B* **2006**, *243*, 494–501.
9. Schmidt, T.; Lischka, K.; Zulehner, W. Excitation-Power Dependence of the Near-Band-Edge Photoluminescence of Semiconductors. *Phys. Rev. B: Condens. Matter Mater. Phys.* **1992**, *45*, 8989–8994.
10. Efros, A. L.; Kharchenko, V. A.; Rosen, M. Breaking the Phonon Bottleneck in Nanometer Quantum Dots: Role of Auger-Like Processes. *Solid State Commun.* **1995**, *93*, 281–284.
11. Pandey, A.; Guyot-Sionnest, P. Slow Electron Cooling in Colloidal Quantum Dots. *Science* **2008**, *322*, 929–932.
12. Hogele, A.; Seidl, S.; Kroner, M.; Karrai, K.; Schulhauser, C.; Sqalli, O.; Scrimgeour, J.; Warburton, R. J. Fiber-Based Confocal Microscope for Cryogenic Spectroscopy. *Rev. Sci. Instrum.* **2008**, *79*, 023709–023707.
13. Osovsky, R.; Cheskis, D.; Kloper, V.; Sashchiuk, A.; Kroner, M.; Lifshitz, E. Continuous-Wave Pumping of Multiexciton Bands in the Photoluminescence Spectrum of a Single CdTe-CdSe Core-Shell Colloidal Quantum Dot. *Phys. Rev. Lett.* **2009**, *102*, 197401–4.
14. García-Santamaría, F.; Brovelli, S.; Viswanatha, R.; Hollingsworth, J. A.; Htoon, H.; Crooker, S. A.; Klimov, V. I. Breakdown of Volume Scaling in Auger Recombination in CdSe/CdS Heteronanocrystals: The Role of the Core−Shell Interface. *Nano Lett.* **2011**, *11*, 687–693.
15. Jarosz, M. V.; Porter, V. J.; Fisher, B. R.; Kastner, M. A.; Bawendi, M. G. Photoconductivity Studies of Treated CdSe Quantum Dot Films Exhibiting Increased Exciton Ionization Efficiency. *Phys. Rev. B: Condens. Matter Mater. Phys.* **2004**, *70*, 195327.
16. Shimizu, K. T.; Neuhauser, R. G.; Leatherdale, C. A.; Empedocles, S. A.; Woo, W. K.; Bawendi, M. G. Blinking Statistics in Single Semiconductor Nanocrystal Quantum Dots. *Phys. Rev. B: Condens. Matter Mater. Phys.* **2001**, *63*, 205316.
17. Galland, C.; Ghosh, Y.; Steinbruck, A.; Sykora, M.; Hollingsworth, J. A.; Klimov, V. I.; Htoon, H. Two Types of Luminescence Blinking Revealed by Spectroelectrochemistry of Single Quantum Dots. *Nature* **2011**, *479*, 203–207.
18. Qin, W.; Shah, R. A.; Guyot-Sionnest, P. CdSeS/ZnS Alloyed Nanocrystal Lifetime and Blinking Studies Under Electrochemical Control. *ACS Nano* **2012**, *6*, 912–918.
19. Marshall, L. F.; Cui, J.; Brokmann, X.; Bawendi, M. G. Extracting Spectral Dynamics from Single Chromophores in Solution. *Phys. Rev. Lett.* **2010**, *105*, 053005.
20. Brokmann, X.; Marshall, L. F.; Bawendi, M. G. Revealing Single Emitter Spectral Dynamics from Intensity Correlations in an Ensemble Fluorescence Spectrum. *Opt. Express* **2009**, *17*, 4509–4517.
21. Bockelmann, U.; Bastard, G. Phonon Scattering and Energy Relaxation in Two-, One-, and Zero-Dimensional Electron Gases. *Phys. Rev. B: Condens. Matter Mater. Phys.* **1990**, *42*, 8947–8951.
22. Muljarov, E. A.; Zimmermann, R. Dephasing in Quantum Dots: Quadratic Coupling to Acoustic Phonons. *Phys. Rev. Lett.* **2004**, *93*, 237401–4.
23. Dekel, E.; Regelman, D. V.; Gershoni, D.; Ehrenfreund, E.; Schoenfeld, W. V.; Petroff, P. M. Cascade Evolution and Radiative Recombination of Quantum Dot Multiexcitons Studied by Time-Resolved Spectroscopy. *Phys. Rev. B: Condens. Matter Mater. Phys.* **2000**, *62*, 11038–11045.
24. Fernee, M. J.; Sinito, C.; Louyer, Y.; Potzner, C.; Nguyen, T.-L.; Mulvaney, P.; Tamarat, P.; Lounis, B. Magneto-Optical Properties of Trions in Non-Blinking Charged Nanocrystals Reveal an Acoustic Phonon Bottleneck. *Nat. Commun.* **2012**, *3*, 1287.
25. Htoon, H.; Malko, A. V.; Bussian, D.; Vela, J.; Chen, Y.; Hollingsworth, J. A.; Klimov, V. I. Highly Emissive Multiexcitons in Steady-State Photoluminescence of Individual "Giant" CdSe/CdS Core/Shell Nanocrystals. *Nano Lett.* **2010**, *10*, 2401–2407.
26. Groeneveld, E.; Delerue, C.; Allan, G.; Niquet, Y.-M.; de Mello Donegá, C. Size Dependence of the Exciton Transitions in Colloidal CdTe Quantum Dots. *J. Phys. Chem. C* **2012**, *116*, 23160–23167.
27. Galland, C.; Högele, A.; Türeci, H. E.; Imamoğlu, A. Non-Markovian Decoherence of Localized Nanotube Excitons by Acoustic Phonons. *Phys. Rev. Lett.* **2008**, *101*, 067402.
28. Htoon, H.; Furis, M.; Crooker, S. A.; Jeong, S.; Klimov, V. I. Linearly Polarized `Fine Structure' of the Bright Exciton State in Individual CdSe Nanocrystal Quantum Dots. *Phys. Rev. B: Condens. Matter Mater. Phys.* **2008**, *77*, 035328.
29. Blokland, J. H.; Claessen, V. I.; Wijnen, F. J. P.; Groeneveld, E.; de Mello Donegá, C.; Vanmaekelbergh, D.; Meijerink, A.; Maan, J. C.; Christianen, P. C. M. Exciton Lifetimes of CdTe Nanocrystal Quantum Dots in High Magnetic Fields. *Phys. Rev. B: Condens. Matter Mater. Phys.* **2011**, *83*, 035304.
30. Gupta, J. A.; Awschalom, D. D.; Efros, A. L.; Rodina, A. V. Spin Dynamics in Semiconductor Nanocrystals. *Phys. Rev. B: Condens. Matter Mater. Phys.* **2002**, *66*, 125307.
31. Godde, T.; Glazov, M. M.; Akimov, I. A.; Yakovlev, D. R.; Mariette, H.; Bayer, M. Magnetic Field Induced Nutation of Exciton-Polariton Polarization in (Cd,Zn)Te Crystals. *Phys. Rev. B: Condens. Matter Mater. Phys.* **2013**, *88*, 155203.
32. Walck, S. N.; Reinecke, T. L. Exciton Diamagnetic Shift in Semiconductor Nanostructures. *Phys. Rev. B: Condens. Matter Mater. Phys.* **1998**, *57*, 9088–9096.